Seasonality of the North Pacific ~~Ocean Desert~~Oligotrophic Gyre area in the past two decades and a modelling perspective for the 21st century

Siyu Meng[1,2,3], Xun Gong[4,5,~~6,~~] Benjamin Webber[3], Manoj Joshi[3], Xiaokun ~~Ding~~[7]Ding[6], Xiang ~~Gong~~[8,9]Gong[7,8], Mingliang Gu[1,2], Huiwang Gao[1,2]

[1]Frontiers Science Center for Deep Ocean Multispheres and Earth System, and Key Laboratory of Marine Environment and Ecology, Ministry of Education of China, Ocean University of China, Qingdao, China.
[2]Laboratory for Marine Ecology and Environmental Sciences, Laoshan Laboratory for Marine Science and Technology, Qingdao, China.
[3]Climatic Research Unit, School of Environmental Sciences, University of East Anglia, Norwich, United Kingdom.
~~[4]Institute for Advanced Marine Research, China University of Geosciences, Guangzhou, China.~~
~~[5]State Key Laboratory of Biogeology and Environmental Geology, Hubei Key Laboratory of Marine Geological Resources, China University of Geosciences, Wuhan, China.~~
~~[6]Shandong Provincial Key Laboratory of~~[4]State Key Laboratory of Physical Oceanography, Institute of Oceanographic Instrumentation, Shandong Academy of Sciences, Ji'nan 250014, China
[5]Shandong Computer ~~Networks~~Science Center, Qilu University of Technology (Shandong Academy of Sciences), ~~Jinan~~Ji'nan 250014, China~~.~~
~~[7]School~~[6]School of Ocean, Yantai University, Yantai, China
~~[8]School~~[7]School of Mathematics and Physics, Qingdao University of Science and Technology, Qingdao, China
~~[9]Qingdao~~[8]Qingdao Innovation Center of Artificial Intelligence Ocean Technology, Qingdao, China

Correspondence to: Xun Gong (gongxun@cug.edu.cn) and Huiwang Gao (hwgao@ouc.edu.cn)

Abstract

As the largest oligotrophic ocean ~~desert~~globally, the North Pacific ~~Ocean Desert (NPOD~~oligotrophic ocean gyre (NPOG) exhibits pronounced ~~variations across~~variability on seasonal, decadal, and centennial time scales. Notably, changes in the seasonality of the ~~NPOD~~NPOG are thought to have larger effects on marine ecosystems than ~~variability~~changes in ~~the~~its annual~~-~~ mean state~~ of the NPOD~~. However, the interannual variability of ~~NPOD~~NPOG seasonality and its response to climate processes remain unclear. Here, we investigate the amplitude of the seasonal cycle in ~~NPOD~~NPOG area and its linkage with climate variability and change. Our results show that the El Niño~~—~~ Southern Oscillation (ENSO) modulated the seasonal maximum of ~~NPOD~~NPOG area in boreal summer, and thus the amplitude of the seasonal cycle during 1998–2021. This is primarily due to ENSO-induced changes in nutrient transport via equatorial upwelling and thermal stratification~~.~~, as well as changes in the chlorophyll-to-carbon ratio in phytoplankton cells (photoacclimation). Future projections based on Coupled Model Intercomparison Project Phase 5 (CMIP5) modelling results and an Elman neural network indicate a significant decrease in the seasonal amplitude of ~~NPOD~~NPOG area by 2100, attributed to the growing seasonal minimum of ~~NPOD~~NPOG area in winter along the anthropogenic increase in atmospheric CO_2. The findings highlight the importance of considering seasonal differences in future research on the interannual variability of ~~ocean~~

~~desert~~oligotrophic gyres and underscore the need for models to distinguish between the effects of climate variability and change.

1 Introduction

~~Ocean deserts are the regions of~~Oligotrophic gyres, characterised by low surface ~~Chlorophyll~~chlorophyll-a ~~(Chl-a)~~ concentrations ~~(less than 0.07 mg m^{-3}), occupying approximately~~and phytoplankton biomass, occupy about 40% of the global ocean~~,~~ and are ~~mainly found~~predominantly situated at subtropical latitudes (McClain et al., 2004). Although phytoplankton biomass is relatively low in these regions, their vast extent and the rapid division rates of phytoplankton cells (Laws, 2013) confer considerable ecological significance. As the largest oligotrophic ocean ~~desert~~globally, the North Pacific ~~Ocean Desert (NPOD~~oligotrophic ocean gyre (NPOG) exhibits variability in area, intensity and location (Meng et al., 2021), coherent with climate dynamics on seasonal (Signorini et al., 2015), decadal (Signorini and McClain, 2012) and centennial (Boyce et al., 2014) time scales. Studies have suggested that the variations of the seasonal cycle in ~~Chl-a and primary production~~chlorophyll concentrations and phytoplankton biomass may have a larger impact on the survival of marine species, and hence the oceanic food web and the ocean carbon cycle, than changes in their annual mean quantities (Lutz et al., 2007; Muñiz et al., 2021), suggesting a need to better quantify any changes in the seasonal cycle of the ~~NPOD~~NPOG.

In previous studies, the ~~NPOD~~NPOG has been quantified by its area and intensity, i.e. spatially averaged ~~Chl-a~~chlorophyll concentration, on the basis of satellite-derived ocean colour datasets (Leonelli et al., 2022; Meng et al., 2021; Wilson and Qiu, 2008), in situ data (Gregg and Rousseaux, 2014), and research cruise observations (Raes et al., 2022). Using satellite observations, McClain et al. (2004) have suggested synchronous variations ~~in the NPOD~~between NPOG intensity and area on seasonal and interannual time scales, indicating that increased ~~NPOD~~NPOG intensity (i.e., lower chlorophyll concentration) usually corresponds to expanded ~~NPOD~~NPOG area. However, extended periods of satellite observation have prompted numerous studies to propose a more pronounced increase in ~~NPOD~~NPOG area than intensity in response to climate processes (Irwin and Oliver, 2009; Meng et al., 2021). Therefore, this study primarily focuses on the variations of ~~NPOD~~NPOG area.

In particular, the seasonal cycle of ~~NPOD~~NPOG area has been linked to nutrient availability in the surface ocean (Behrenfeld et al., 2006; Henson et al., 2013; Kwiatkowski et al., 2017). In boreal summer, higher sea surface temperatures (SSTs) inhibit the mixing between surface water and the subsurface nutrient-rich water, by enhancing vertical stratification and shoaling the mixed layer depth (MLD) (Signorini et al., 2015). As a result, the reduced availability of nutrients in the surface waters limits the growth of phytoplankton, leading to lower ~~Chl-a~~chlorophyll concentrations and ~~NPOD~~NPOG area expansion in summer. Conversely, in winter, the mixed layer deepens~~,~~ due to relatively low SSTs, entraining nutrient-rich water and ~~causing~~leading to increased chlorophyll ~~blooms~~and NPOG area contraction (Mao et al., 2020).

In addition, changes in light availability can also influence chlorophyll concentrations through phytoplankton photoacclimation. Even if nutrient supply and phytoplankton biomass remain unchanged, a shallower mixed layer or higher

surface irradiance is expected to decrease chlorophyll concentration, as phytoplankton lower their pigment content in response to higher average light levels within the mixed layer (Behrenfeld et al., 2005, 2016).

Studies have suggested that the variation of ~~Chl a~~chlorophyll concentration in subtropical ocean is ~~likely driven by~~also linked with basin-wide climate processes. For example, the El Niño~~–~~–Southern Oscillation (ENSO), characterized by the variability over 2–7 years, can regulate the nutrient transfer to the upper ocean via changes in ocean horizontal advection and upwelling (Racault et al., 2017). Over longer timescales, ~~the Pacific Decadal Oscillation (PDO) reflects variability in the patterns of ocean circulation and SSTs, which are associated with changes in the nutrients availability and Chl a concentrations in NPOD (Martinez et al., 2009; Meng et al., 2021). In parallel,~~ climate warming has been shown to intensify ~~the~~ thermal stratification and nutrient limitation in the upper ocean ~~and~~, and to alter phytoplankton pigment content through photoacclimation, consequently ~~leads~~leading to ~~NPOD~~NPOG expansion on a time scale of several decades (Behrenfeld et al., 2016; ~~(~~Henson et al., 2010; Lewandowska et al., 2014; Meng et al., 2021). Hence, to achieve a comprehensive understanding of how ~~NPOD~~NPOG seasonality responds to the dual influences of interannual climate variability and long-term climate change, it is crucial to investigate the ~~NPOD~~NPOG seasonality across different time scales.

While previous research has acknowledged the potential effects of chlorophyll and phytoplankton seasonality on marine ecosystems and the carbon cycle, the variation in the seasonality of ~~NPOD~~NPOG, the ocean with the lowest ~~phytoplankton~~chlorophyll level globally, and its response to climate processes remain unclear. In this study, we aim to better understand and quantify the variation in the amplitude of the seasonal cycle (i.e. the difference between maximum and minimum in the annual cycle) in ~~NPOD~~NPOG area. To do this, we use satellite ~~Chl a~~chlorophyll data during 1998–2021~~,~~ and ~~also evaluate~~project future ~~projections~~changes for the 21st century based on an Elman Neural Network (ENN) model and ~~results~~model output from the Coupled Model Intercomparison Project Phase 5 (CMIP5) (Taylor et al., 2012).

2 Data and Methods

2.1 Data

2.1.1 Chlorophyll-a observations

In this study, the ~~NPOD~~NPOG is defined as the region within which the ocean surface ~~Chl-a~~chlorophyll concentration is less than 0.07 mg m^{-3}, following McClain et al. (2004) and Polovina et al. (2008). We obtain ~~Chl-a~~chlorophyll concentration data from Sea-viewing Wide Field-of-View Sensor (SeaWiFS) and Moderate Resolution Imaging Spectroradiometer (MODIS/Aqua) ocean colour observations (NASA OBPG, 2014). Here, a 13 day running-mean and 11–grids spatial smoothing are utilized to fill in the missing values of ~~Chl-a~~chlorophyll data due to cloud coverage (Cole et al., 2012). Then, the SeaWiFS dataset from 1998 to 2007 and MODIS dataset from 2003 to 2021 are merged to form a continuous dataset of monthly ~~Chl-a~~chlorophyll observation at 9 km spatial resolution from 1998 to 2021. To achieve this, a cross-calibration is performed at each grid point based on the overlapping period in the SeaWiFS and MODIS-Aqua datasets (Fig. S1). Overall, there are 1719140 pairs of concurrent ~~Chl-a~~chlorophyll concentration data in ~~NPOD~~NPOG region over the 5 years overlapping period, and the two datasets present ~~a~~an R-squared coefficient of 0.78 with offset of 0.0025, suggesting a strong coherence between the SeaWiFS and the MODIS datasets (Fig. S1). The merged database has been validated ~~in Meng et al. (2021)~~ and used to analyse decadal variability ~~in~~of the ~~NPOD~~NPOG in Meng et al. (2021).

2.1.2 Physical datasets

All observational and reanalysis data used in this study are listed in Table S1. Specifically, the Optimum Interpolation SST data from National Oceanic and Atmospheric Administration (NOAA) (Reynolds, 1988), sea surface height data from Global Ocean Data Assimilation System (GODAS) provided by NOAA Physical Sciences Division, MLD data from the Simple Ocean Data Assimilation version 3 (SODA3) reanalysis dataset (Carton et al., 2018), downward solar radiation and precipitation rate data from European Center for Medium Range Weather Forecasting (ECMWF) ERA5 reanalysis ~~dataset~~

(Hersbach et al., 2019), and wind stress data from ECMWF ORAS5 (Zuo et al., 2019) are used to explore the response of NPODNPOG seasonality to physical climate variability. Wind stress curl is calculated from the ORAS5 wind stress to investigate the role of wind-driven downwelling in the NPODNPOG. Furthermore, ocean horizontal velocity components, temperature and salinity data from the SODA3 reanalysis data from 1998 to 2015 are used to force a one-dimensional K-profile parameterization (KPP) ocean model (Large et al., 1994) to evaluate ocean vertical mixing process at each grid point in the NPODNPOG area. Nutrient concentration data (Nitrate + Phosphatenitrate + phosphate) from World Ocean Atlas 2005 (Levitus, 2006) is combined with K-profile parameterizationKPP analysis to calculate nutrient fluxes across 10 m depth into the surface ocean (Text S1). The ENSO signal is represented by the Niño 3.4 index, which is obtained from NOAA Physical Sciences Laboratory (Rayner et al., 2003) and calculated by using the HadISST1 dataset.

2.1.3 Phytoplankton biomass and light conditions within mixed layer

In this study, we emphasise that surface chlorophyll concentration should not be interpreted as phytoplankton biomass and is even less indicative of primary productivity. Chlorophyll concentration can vary not only through changes in phytoplankton biomass but also through changes in intracellular pigment content in response to light conditions (photoacclimation). To investigate these effects, we incorporated two additional datasets. First, we use particulate organic carbon (POC) data from MODIS and calculate phytoplankton carbon to estimate phytoplankton biomass following the approach of Behrenfeld et al. (2005), from which we also derive chlorophyll-to-carbon ratios (Chl:C). Second, we calculate mixed layer light availability, defined as the average photosynthetically available radiation (PAR) within the mixed layer, following Behrenfeld et al. (2005). This metric represents the light environment experienced by phytoplankton in the upper ocean and is a key driver of photoacclimation. Together, these datasets allow us to distinguish changes in chlorophyll concentration driven by phytoplankton biomass from those resulting from changes in the Chl:C ratio induced by light conditions.

2.1.4 Climate model output

For the projections of the NPODNPOG area in the 21st century, we apply the ENN machine learning model to 7 CMIP5 simulations (Table S2) based on the Representative Concentration Pathway 8.5 (RCP 8.5) scenario (Taylor et al., 2012). RCP 8.5 experiment simulates a climate change scenario which is forced by prescribed greenhouse gas and other natural forcings, and the radiative forcing value is projected to rise toreach 8.5 W m^{-2} by 2100. It provides an insight into the climate impacts of high-end greenhouse gas emission pathways (Moss et al., 2010; Schwalm et al., 2020). The CMIP5 modelling outputs provide data at monthly resolution from 2006 to 2100. These outputs are standardized by converting them to Z-scores before being input into the ENN model. Further description of the CMIP5 data is provided in Text S2.

2.2 Elman Neural Network

A key aim of this study is to project the NPODNPOG area seasonality in a future climate change scenario. However, the overall underestimation of Chl achlorophyll concentration in subtropical gyres in Earth System Models (ESMs) (Séférian et al., 2013) precludes using such models to identify the boundary and area of the NPODNPOG (Fig. S2c). Compared with Chl achlorophyll concentration, the physical properties of the ocean and atmosphere that are key factors regulating the

~~NPOD~~NPOG variation, e.g. SST and wind stress curl, are better represented in the ~~NPOD~~NPOG region (Fig. S3). Therefore, an ENN model is combined with physical variables from CMIP5 modelling outputs (models listed in Table S2 and more details in Text S2) to make projections of ~~NPOD~~NPOG area over the 21st century. ENN (Elman, 1990) is a typical recurrent neural network which reuses past information as inputs to predict the next or future states. Compared to traditional neural networks consisting of input, hidden and output layers, ENN adds a context layer to pass the information from the last network iteration to the current iteration. Thus, ENN is more suitable to model temporal sequences especially with strong periodic variations like the seasonality of ~~the NPOD~~NPOG area.

Although ENN is an effective method to predict time series, when ~~NPOD~~NPOG area variation exhibits a high degree of ~~nonstationary~~nonstationarity due to the dual effects of climate variability and change, the accuracy and robustness of ENN may be reduced (Stock et al., 2018). Therefore, we use the time series of SST, wind stress curl and solar radiation in ~~NPOD~~NPOG region, based on the observation and reanalysis data, as the input data of ENN, and the time series of ~~NPOD~~NPOG area as the output data to evaluate the ENN performance. These input variables are selected by a sensitivity test that assesses ENN performance with different input configurations (Table S3). Here, 69% of the ~~NPOD~~NPOG area time series is used for ENN training, and 31% of the ~~NPOD~~NPOG area time series is used to ~~verify~~validate the ~~error~~difference between the ~~NPOD~~NPOG areas predicted by ENN and observed by satellite. As shown in Fig. S4, the relative error of ENN prediction is only 7.06%, indicating the good performance of ENN in projecting ~~NPOD~~NPOG area (Mean Absolute Error = 1.75 10^6 km^2, Root Mean Square Error = 2.46 10^6 km^2, R-squared = 0.82). Moreover, the ENN results are compared with the ~~NPOD~~NPOG area simulations by three ESMs, CMCC-CESM, CNRM-CM5 and IPSL-CM5A, which are best able to capture observed ~~Chl-a~~chlorophyll distribution among CMIP5 models (Fu et al., 2022). Although the seasonal cycles of ~~NPOD~~NPOG area are well simulated in both ESMs and ENN (Figs. S2b, S4), the systematic biases of ~~NPOD~~NPOG area and location in ESMs are ~~very~~ substantial, with the average simulated ~~NPOD~~NPOG area being more than double the observed area (Fig. S2a,~~-~~c).

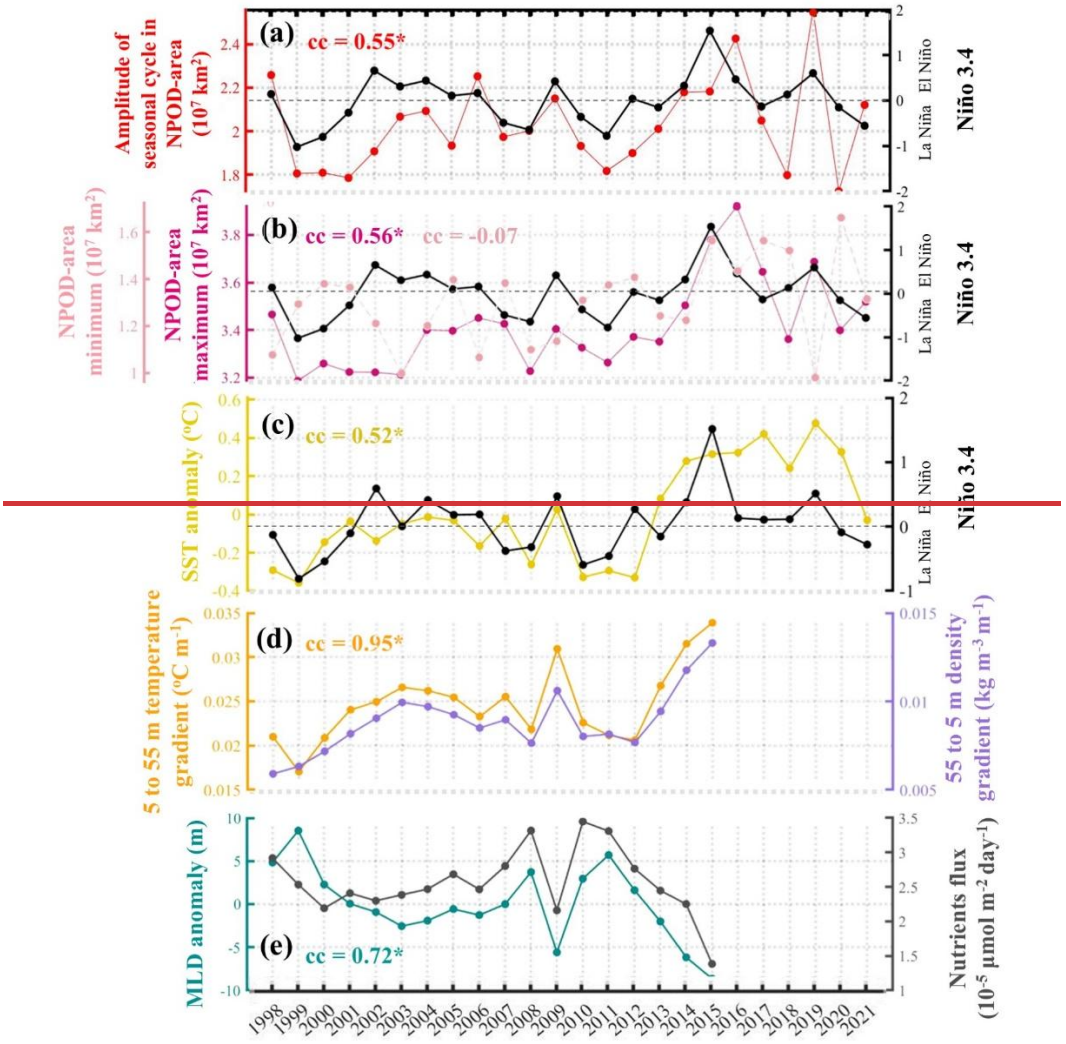
(a) cc = 0.55*
Amplitude of seasonal cycle in NPOD-area (10^7 km^2)
Niño 3.4
La Niña
El Niño
(b) cc = 0.56*
cc = -0.07
NPOD-area minimum (10^7 km^2)
NPOD-area maximum (10^7 km^2)
(c) cc = 0.52*
SST anomaly (°C)
(d) cc = 0.95*
5 to 55 m temperature gradient (°C m^-1)
55 to 5 m density gradient (kg m^-3 m^-1)
(e) cc = 0.72*
MLD anomaly (m)
Nutrients flux (10^-5 µmol m^-2 day^-1)
1998
1999
2000
2001
2002
2003
2004
2005
2006
2007
2008
2009
2010
2011
2012
2013
2014
2015
2016
2017
2018
2019
2020
2021

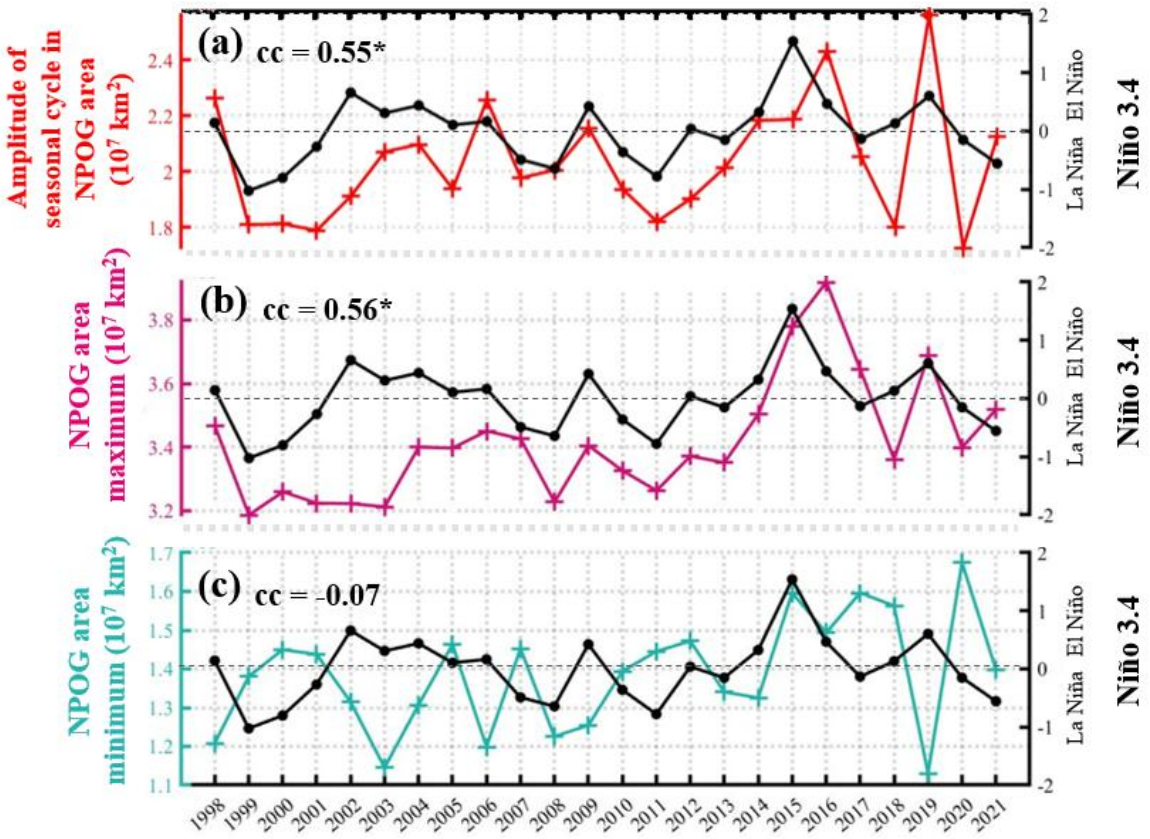

Figure 1. Interannual variation in ~~NPOD~~NPOG area seasonal cycle as a response to ENSO. (a) Amplitude of the seasonal cycle in ~~NPOD~~NPOG area (~~left axis~~red) and Niño 3.4 index (~~right axis~~black) in 1998–2021. (b) ~~NPOD~~NPOG area seasonal maximum (~~dark red, solid) and minimum (light red, dashed~~magenta) and Niño 3.4 index (black) in 1998–2021. ~~(c-e) SST anomaly in NPOD and Niño 3.4 index (c), temperature gradient and density gradient of 5 to 55 m (d), MLD anomaly and upward nutrient flux from vertical mixing (e) in NPOD in each summer half year. "cc" represents the correlation coefficient, "*" represents the p-value less than 0.01. All variables in (c-e) are averaged within the fixed NPOD region, which is determined by the multi-year average of Chl-a data.~~

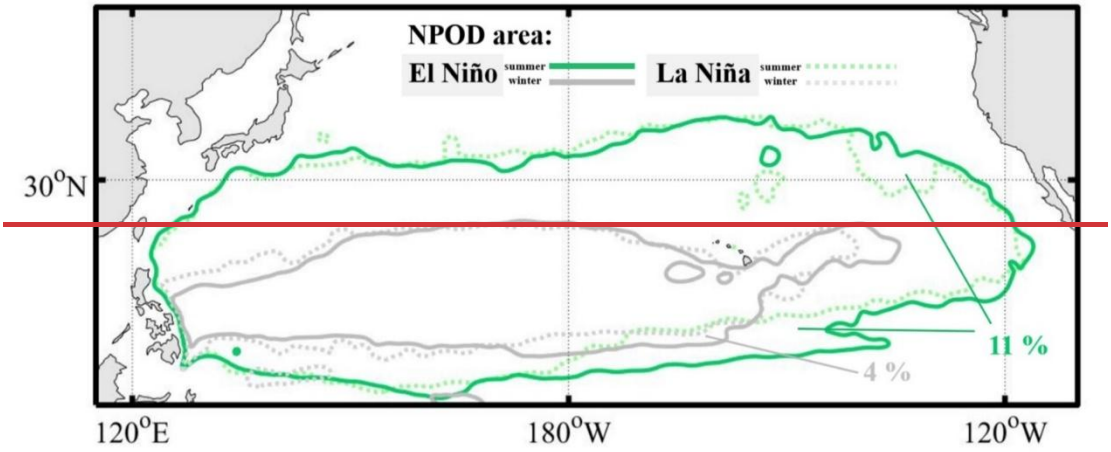

205 (c) NPOG area ~~Figure 2. The boundaries of NPOD~~ seasonal ~~maximum area~~minimum (green~~–~~) and Niño 3.4 index (black) in 1998–2021. The lines marked with "+" correspond to the left y-axis, while those marked with "•" correspond to the right y-axis.

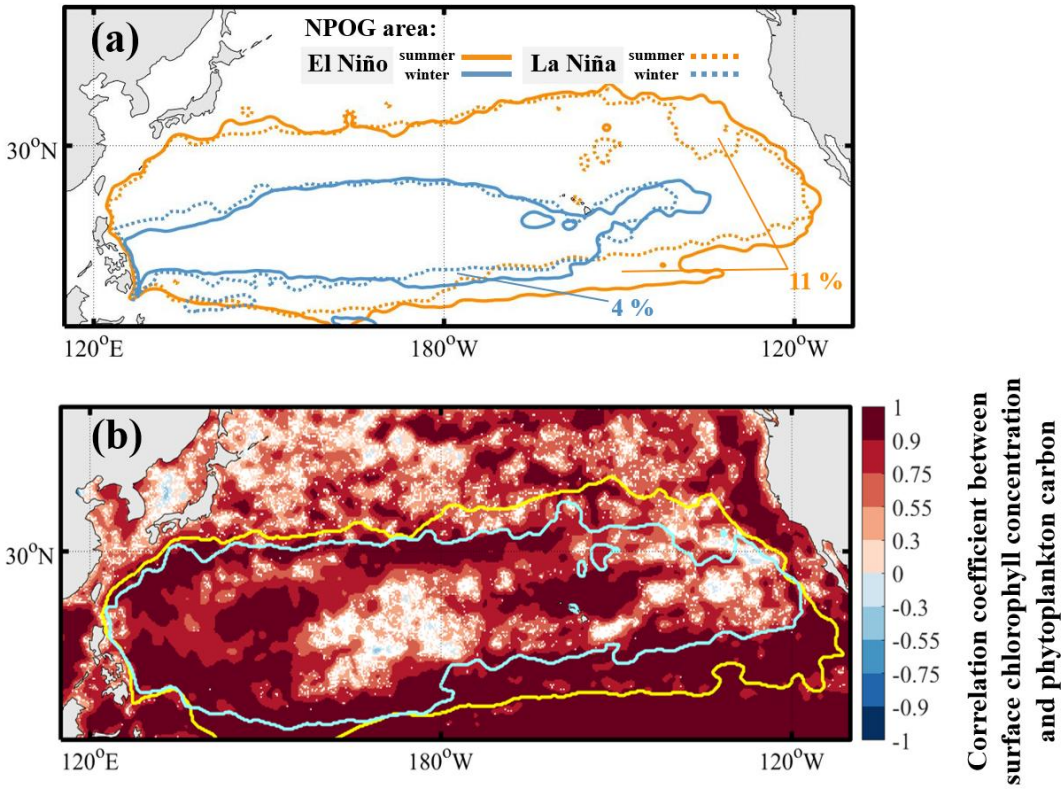

Figure 2. Interannual variation in the NPOG boundary. (a) Boundaries of the seasonal maximum (yellow) and minimum ~~area (grey lines) in~~ (blue) NPOG areas during El Niño (dark ~~colour~~, solid) and La Niña (light ~~colour~~, dashed) years. ~~The~~

~~percentages~~Percentages indicate the relative differences in ~~the NPOD's~~ seasonal maximum (yellow) and minimum (blue) areas between El Niño and La Niña years~~, relative to~~ compared with the climatological mean. (b) Boundaries of the largest (yellow) and smallest (light blue) extents of seasonal maximum NPOG area across different years. Colour shading represents the correlation coefficient between the interannual variations of summer surface chlorophyll concentration and phytoplankton carbon.

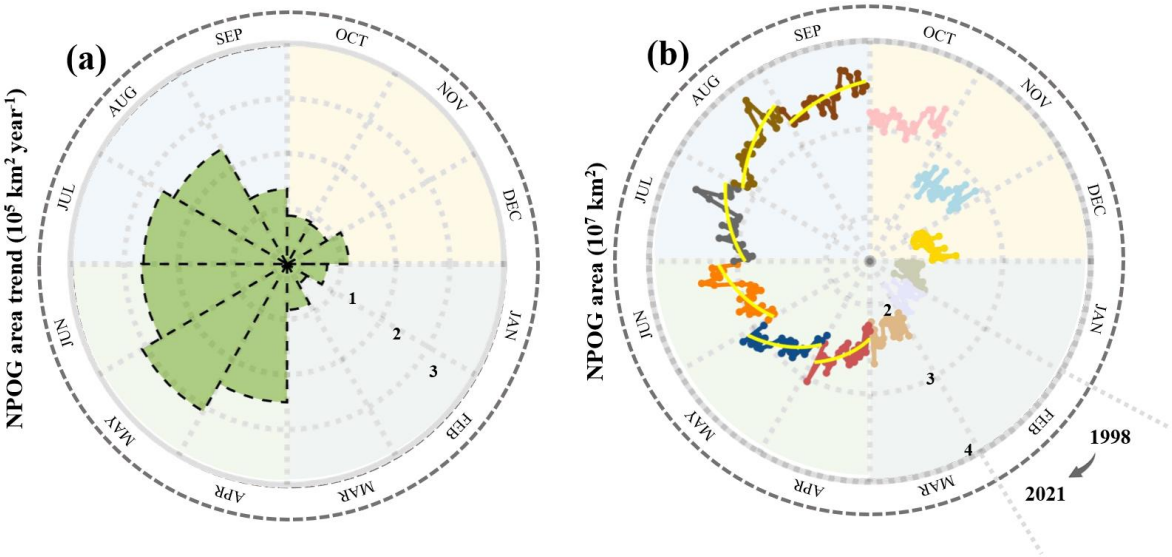

Figure 3. Interannual variations of NPOG area in different months. (a) Trends of NPOG area expansion in 1998–2021 for specific month, according to the linear-fitted regressions of NPOG area time series as shown in (b). (b) Time series of NPOG area in 1998-2021 for specific month. The yellow lines in (b) represent the linear regressions that pass the significance test at the 0.01 level.

3 ENSO-induced variation in the ~~NPOD~~NPOG seasonality

3.1 The variation in seasonal cycle of ~~NPOD~~NPOG area as a response to ENSO

The amplitude of the seasonal cycle in ~~NPOD~~NPOG area displays interannual variability without a significant trend during 1998–2021 (Fig. S5a), strongly correlated with ENSO (using the Niño 3.4 index, Fig. 1a). On average, the ~~NPOD~~NPOG area seasonal amplitude ~~of the~~in El Niño years (2002, 2004, 2015, 2016 and 2019) is ~ 16% larger than for the La Niña years (1999, 2000, 2007, 2008 and 2011).

ENSO drives the variation in ~~NPOD~~NPOG area seasonal cycle via its effect on the seasonal maximum of ~~NPOD~~NPOG area~~,~~ (Fig. 1b), with little impact on the seasonal minimum of ~~NPOD~~NPOG area (Fig. ~~1b~~1c). Even when we use the Niño 3.4 index in January, which corresponds to the month of ~~NPOD~~NPOG area minimum, its correlation with the seasonal minimum in ~~NPOD~~NPOG area remains insignificant (Fig. S5b). Geographically, the enhanced seasonal cycle in ~~NPOD~~NPOG area in El Niño years is mainly caused by the ~~NPOD~~NPOG expansion to the southeast and northeast in boreal summer when the ~~NPOD~~NPOG area reaches its seasonal maximum (~~green~~yellow lines in Fig. ~~2~~2a). Meanwhile, the ~~NPOD~~NPOG area in boreal winter doesn't change much between El Niño and La ~~Nina conditions~~Niña years, with comparably low values in both

ENSO phases (~~grey~~blue lines in Fig. ~~2~~2a). Therefore, the interannual variation in the seasonal amplitude of ~~NPOD-~~NPOG area shows dependence on the maximal area in summer, and this variation can be linked to ENSO.

Previous studies have reported the fast expansion of ~~NPOD~~NPOG over the past two decades based on annual~~-~~ mean data (Boyce et al., 2014; Meng et al., 2021), but our findings show that the expansion rate is season-dependent. As shown in ~~Fig~~Figs. 3 and S6, the ~~NPOD~~NPOG expansion rate in summer, 2.7 10^5 km^2 $year^{-1}$, is considerably larger than either in winter, 0.7 10^5 km^2 $year^{-1}$, or for the annual~~-~~ mean rate of 1.35 10^5 km^2 $year^{-1}$ (Meng et al., 2021). Although the pronounced ~~NPOD~~NPOG expansion in summer may influence the ~~NPOD-~~NPOG area seasonal cycle, the trend of ~~NPOD-~~NPOG area seasonal amplitude from 1998 to 2021 is not statistically significant in the presence of ENSO (Fig. S5a). Therefore, longer timescales of observations may be needed to detect a significant change in ~~NPOD~~NPOG seasonality (Henson et al., 2010; Tian and Zhang, 2024). Moreover, the interannual variation of the ~~NPOD~~NPOG area, represented by its standard deviation (Fig. ~~S6~~S7), is relatively large in summer, which further explains why the interannual variation of ~~NPOD-~~NPOG area seasonal cycle depends on the summer maximal ~~NPOD~~NPOG area.

3.2 ENSO-induced variations in ocean physics and their impact on ~~NPOD~~NPOG area

To investigate the influence of ENSO on ~~NPOD seasonality~~interannual variations in the summer NPOG area, we define our study region as the area spanning the range between the interannual maximum and minimum extent of the NPOG seasonal maximum area (between the yellow and blue lines in Fig. 2b). Within this region, surface chlorophyll variations largely determine the interannual variations in the NPOG area seasonal maximum and NPOG area seasonal cycle. We then analyse the coherence between the Niño 3.4 index and ~~various~~a set of physical parameters, averaged within ~~the NPOD~~this region, that represent key processes ~~influencing NPOD~~shaping the NPOG area ~~(~~, including SST, MLD, upward nutrient flux to ~~ocean~~the surface, and the temperature ~~gradient~~ and density ~~gradient~~gradients over 5 ~~to~~ 55 m depth~~;~~ (Fig. ~~1~~4). All ~~data~~variables are averaged over the boreal summer half year (April–September), which ~~we have~~has been shown to ~~determine~~dominate the interannual variation of the ~~NPOD~~NPOG area seasonal ~~amplitude.~~ cycle.

In El Niño years, higher SSTs and the associated ~~increased~~increase in the vertical temperature gradient between 5 ~~to~~and 55 m lead to ~~a~~ strengthened thermal stratification (Fig. ~~1c, d). Accordingly, thermal~~4a,b). The enhanced stratification in the upper ocean shoals the MLD and inhibits upward nutrient transport (Fig. ~~1e), finally~~4c), leading to ~~Chl a~~concurrent reductions in phytoplankton biomass and chlorophyll concentration ~~reduction~~(Fig. 4d), and ~~NPOD area~~the expansion ~~in El~~of the NPOG area during El Niño years. ~~Therefore, the~~These ENSO-related SST variations thus represent a ~~dominant~~ indirect ~~ocean~~ thermal effect on the ~~NPOD area in the~~ summer ~~half year~~NPOG area and ~~thus on~~, consequently, the amplitude of ~~the NPOD~~NPOG area seasonal cycle.

Our results show that chlorophyll and phytoplankton carbon are closely related in this region (Fig. 2b), although variations in surface chlorophyll are not solely driven by nutrient-induced changes in biomass. Our estimates of mixed layer light levels indicate that ENSO can also affect the MLD and the average light availability within the mixed layer, inducing the photoacclimation response in phytoplankton that alters Chl:C ratio and thereby surface chlorophyll concentration (Fig. 4e).

Notably, variations in surface chlorophyll caused by photoacclimation do not necessarily reflect changes in phytoplankton biomass or primary production. For example, an increase in light availability within the mixed layer can reduce Chl:C, leading to lower surface chlorophyll while vertically integrated biomass and primary production remain unchanged or even increase. Reduced surface chlorophyll also lowers the light attenuation coefficient, allowing more light to penetrate deeper layers (Manizza et al., 2005; Meng et al., 2024), potentially further supporting higher vertically integrated phytoplankton biomass and primary production.

Furthermore, ENSO can impact the ~~NPOD~~NPOG area seasonal maximum locally by regulating equatorial upwelling. In El Niño years, suppression of equatorial upwelling and a decrease of westward advection of nutrient-rich water result in ~~Chl a~~chlorophyll decline in the eastern equatorial Pacific (Fig. ~~S7b,~~ S8b,c) and ~~NPOD~~NPOG expansion in its southern region (Fig. ~~2~~2a). As a result, ENSO signals can only regulate the interannual variation of ~~NPOD~~NPOG area in summer when ~~NPOD~~NPOG expands to its seasonal maximum and reaches the equatorial region (Fig. ~~2~~2a).

However, this ~~summer~~ pronounced summer ENSO impact on ~~NPOD~~NPOG is inconsistent with existing evidence, which shows that the ENSO signals have the largest impact on ocean physics in boreal winter and early spring (An and Wang, 2001). Here, one possible reason is that ENSO-induced ~~upwelling~~thermal and ~~SST~~physical anomalies persist through the spring and summer (Jacox et al., 2015; Wu and Kirtman, 2005). This is combined with the constraint that ~~NPOD~~NPOG area can only expand in summer to the central and eastern equatorial Pacific where there are significant ENSO signals (Fig. ~~2~~2a).

Notably, ~~Chl a~~chlorophyll concentrations show low interannual variability in the western and northwestern regions of the ~~NPOD~~NPOG as a response to ENSO (Fig. ~~2~~2a). In the western ~~NPOD~~NPOG, the boundaries of the ~~ocean desert~~oligotrophic region are constrained by the relatively eutrophic inshore regions along the western boundary, where ~~Chl a~~chlorophyll distributions exhibit negligible interannual variations. In the northwestern ~~NPOD~~NPOG, the interannual variability in ~~ocean desert~~oligotrophic gyre boundaries, especially in summer (Fig. ~~2~~2a), is governed by the Kuroshio extension system, characterized by its pronounced eddy activity and high ~~Chl a~~chlorophyll concentrations (Itoh et al., 2015). The ocean dynamics and ~~Chl a~~chlorophyll level of the Kuroshio extension are predominantly regulated by low-frequency climate variability such as Pacific Decadal Oscillation (PDO) (Lin et al., 2014). Therefore, the western and northwestern ~~NPOD~~NPOG demonstrate insignificant interannual variability in response to ENSO signal.

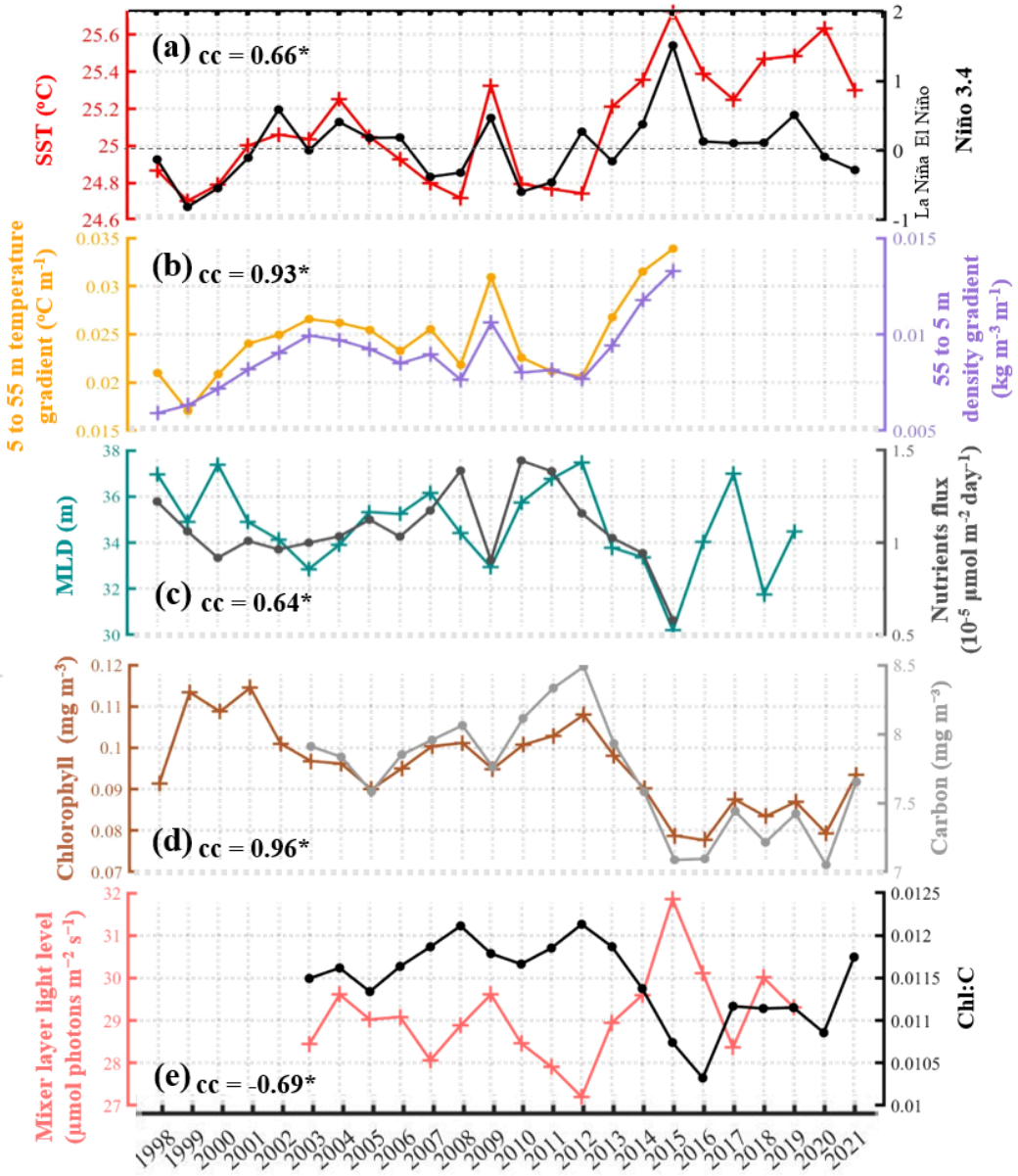

Figure 4. Effects of ENSO on the interannual variations in NPOG area. Interannual variations in (a) SST and Niño 3.4 index, (b) temperature and density gradients between 5 and 55 m, (c) MLD and upward nutrient flux from vertical mixing, (d) sea surface chlorophyll concentration and phytoplankton carbon, and (e) mixed layer light level and Chl:C. All variables are averaged over the summer half year (April–September) within the region bounded by the yellow and blue lines in Fig. 2b. "cc" denotes the correlation coefficient between paired variables, and "*" indicates $p < 0.01$. The lines marked with "+" correspond to the left y-axis, while those marked with "•" correspond to the right y-axis.

3.3 Impact of ENSO on the Seasonal Peak Timing of Chlorophyll-a ~~seasonal bloom~~ in ~~NPOD~~NPOG

We have also identified a connection between ENSO and ~~Chl-a~~chlorophyll seasonality ~~within~~in the ~~NPOD~~central NPOG region, as a coinciding phenomenon along with the variations in ~~NPOD~~NPOG area seasonality. Here, ~~Chl-a~~chlorophyll seasonality is characterized by the timing of its ~~bloom~~annual peak, which is ~~defined by~~ the ~~time~~month when ~~Chl-a~~chlorophyll reaches its ~~annual peak~~seasonal maximum value (Fig. ~~4).~~ 5).

In most ~~NPOD~~NPOG regions, ~~Chl-a blooms in~~chlorophyll peaks during the winter half year (October–March) (Fig. ~~4a), which is~~ 5a), consistent with weaker ~~ocean~~ stratification ~~in winter.~~and deeper mixed layers that enhance nutrient supply, together with reduced light levels within the mixed layer that elevate Chl:C. However, in the central area of the ~~NPOD, Chl-a blooms~~NPOG, chlorophyll peaks in the summer half year (April–September), more specifically in May–July. After cataloguing ~~Chl-a~~chlorophyll seasonal cycles in El Niño and La Niña years, we find that the summer ~~Chl-a bloom~~chlorophyll peak in the central ~~NPOD~~NPOG only occurs in La Niña years (Fig. ~~4c~~5c). During La Niña conditions, the chlorophyll peak is likely associated with the deepening of the mixed layer, which reduces light availability within the mixed layer and thereby elevates the Chl:C ratio (Fig. S9). Study has suggested wind-driven mixing should also be considered when analysing the summer weak nutrient supply induced by enhanced vertical stratification in the subtropical gyre (Lozier et al., 2011). Here, we show that the northeasterly wind anomalies north of the equator in ~~summer leads~~La Niña years can also lead to stronger zonal wind stress and wind stress curl (Fig. S10d) (Chow et al., 2019; Feng et al., 2020)~~ in the central NPOD area (Fig. S8d). Therefore, nutrients~~, which can ~~be transported to the surface ocean during the pre-bloom period due to enhanced~~further enhance nutrient supply through wind-induced ~~deep~~ mixing and ~~horizonal nutrient~~ horizontal transport (Toyoda and Okamoto, 2017; Wilson et al., 2013), ~~finally leading~~potentially providing a secondary contribution to ~~summer Chl-a bloom~~the observed local chlorophyll peak (Fig. ~~S8b).~~ S10b).

Previous studies have attributed some ~~Chl-a bloom events observed~~ summertime chlorophyll increases in the oligotrophic Pacific to nitrogen fixation (Villareal et al., 2012; Wilson and Qiu, 2008)~~. However, the location of the Chl-a blooms in~~, but these ~~studies is situated to the~~peaks were located farther east ~~of the Chl-a blooms~~than those in Fig. ~~4a. Moreover, previous research using~~5a, and cruise ~~data has suggested~~ observations suggest nitrogen fixation exerts an insignificant impact ~~of nitrogen fixation~~ on summer ~~Chl-a blooms~~chlorophyll in the ~~NPOD region~~NPOG (Villareal et al., 2011). Therefore, nitrogen fixation is unlikely to ~~be the main cause of~~explain the summer ~~Chl-a bloom~~chlorophyll peak in this ~~study. Overall, our results suggest that the two key indicators of NPOD seasonally, i.e. NPOD area seasonal amplitude and Chl-a bloom, can be both linked to ENSO via equatorial upwelling, vertical stratification, wind induced horizontal transport and mixing processes~~region.

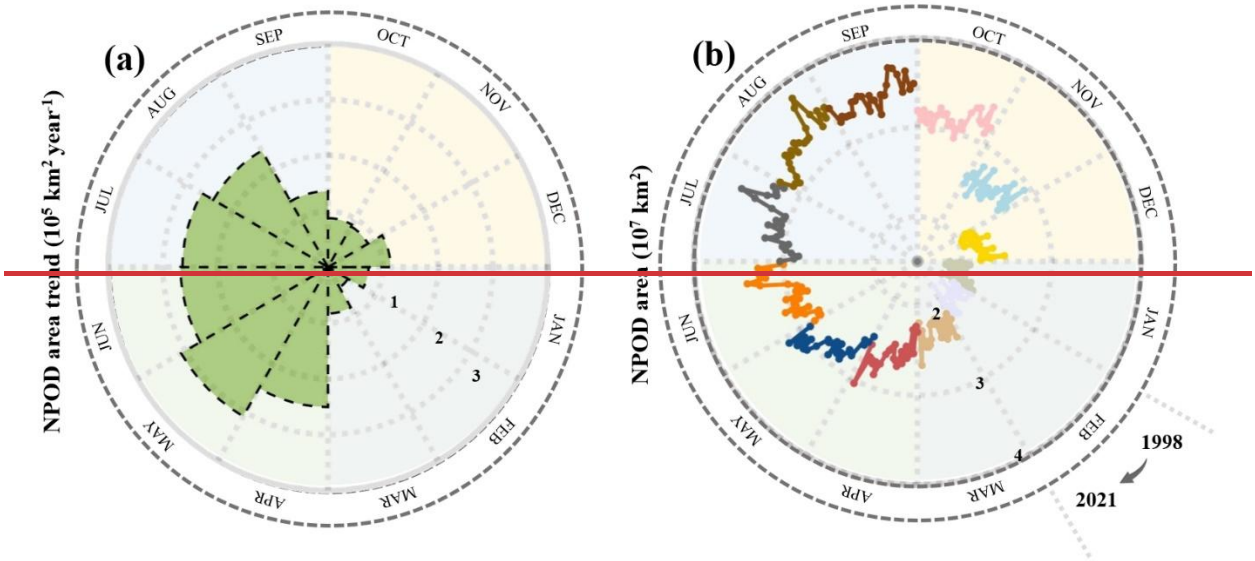
(a)
(b)
SEP
OCT
NOV
DEC
JAN
FEB
MAR
APR
MAY
JUN
JUL
AUG
1
2
3
4
1998
2021
NPOD area trend (10^5 km^2 year^-1)
NPOD area (10^7 km^2)

325

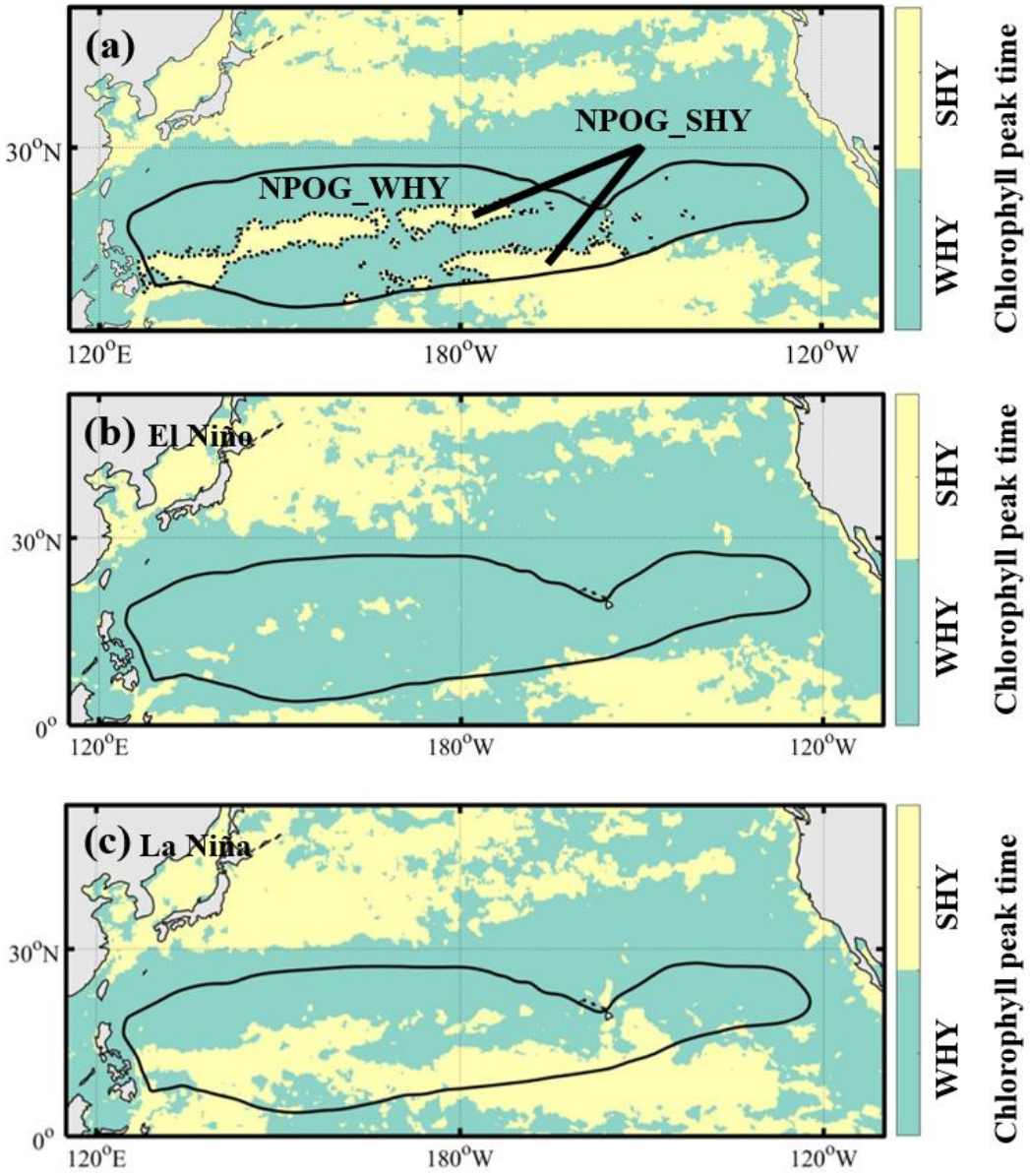

~~Figure 3. Interannual variations of~~ NPOD area in different months. (a) Trends of NPOD area expansion in 1998–2021 for specific month, according to the linear-fitted regressions of NPOD-area time series as shown in (b). (b) Time series of NPOD area in 1998–2021 for specific month.

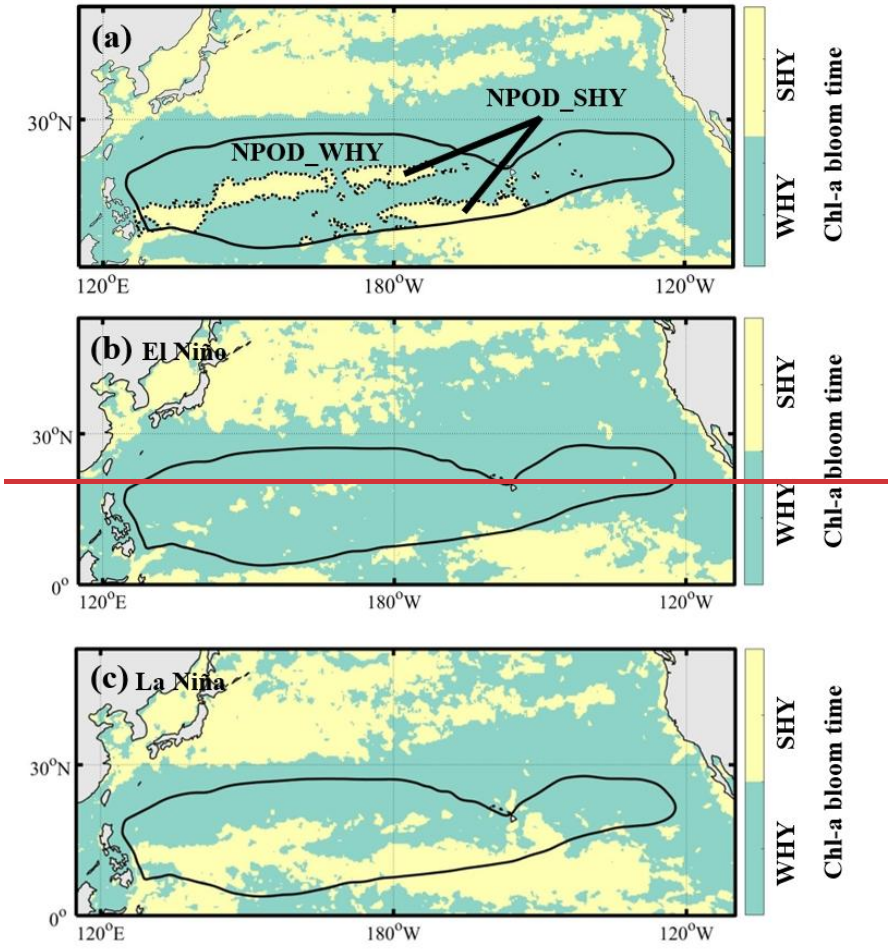

Figure ~~4. Chl-a bloom~~5. Chlorophyll peak time in North Pacific. (a) ~~NPOD~~NPOG region is categorized to ~~NPOD~~NPOG WHY (WHY for Winter Half Year, October–March) and ~~NPOD~~NPOG SHY (SHY for Summer Half Year, April–September) based on the climatological ~~Chl-a bloom~~chlorophyll peak time. (b-c) ~~Chl-a bloom~~chlorophyll peak time in El Niño years (b) and La Niña years (c). The black contour represents the multi-year mean NPOG boundary.

4 Projection of the ~~NPOD~~NPOG seasonality during the 21st century

4.1 Predicting ~~NPOD~~NPOG seasonality with ENN model

To understand the response of the ~~NPOD~~NPOG seasonality to future climate change, an ENN model driven by CMIP5 multi-model mean output is used to predict the amplitude of the ~~NPOD~~NPOG area seasonal cycle during the 21st century. Based on a sensitivity test of ENN performance with different input configurations (Table S3), we select SST, wind stress curl and solar radiation as the optimal input data to the ENN. The selection of these variables is also in line with the discussion in Sect. 3 and the findings of Meng et al. (2021), which ~~specifically highlight~~emphasize the ~~determining impact~~role of SST ~~variations on~~ in modulating ocean vertical stratification and ~~NPOD area~~the influence of solar radiation on phytoplankton photoacclimation.

We evaluate the ENN-predicted variations in amplitude of seasonal cycle in ~~NPOD~~ NPOG area, as well as the ~~NPOD~~NPOG area maximum and minimum, from 2006 to 2100 (Fig. ~~5~~6). During the first half of the century (2006–2048), both the summer maximum and the winter minimum of ~~NPOD~~NPOG area are predicted to expand (Fig. ~~5b~~6b) due to higher SST and thus enhanced upper ocean stratification (Yamaguchi and Suga, 2019). This results in a relatively gradual change in the amplitude of the ~~NPOD~~NPOG area seasonal cycle (Fig. ~~5a~~6a), largely consistent with the insignificant trend in observations (Fig. S5a). However, a notable shift occurs in the latter half of the century (2049–2100), where the expansion of the ~~NPOD~~NPOG area seasonal maximum comes to a halt, while the expansion of the seasonal minimum continues. This is likely because the expanded boundary of the ~~NPOD~~NPOG maximal area is affected by other dynamical processes, such as eddy-induced mixing and upwelling at the margins of subtropical gyre (Barber and Chavez, 1983; Pennington et al., 2006), and confined in the more stably stratified subtropical gyre which prevents further expansion of the ~~NPOD~~NPOG area maximum. Overall, the rate at which the seasonal minimal ~~NPOD~~NPOG area expands is significantly higher than the seasonal maximal area, especially in the second half of the century, leading to a decreasing trend of the ~~NPOD~~NPOG area seasonal amplitude (Fig. ~~5a).~~ 6a).

We note that the input variables are not entirely independent, as SST, wind stress curl, and solar radiation all interact to influence the MLD, nutrient availability, and the light level within the mixed layer, highlighting the complex coupling between physical forcing and biological responses. However, this interdependence is not a major concern here, because the ENN is designed to capture the combined, non-linear effects of correlated predictors, and our sensitivity tests (Table S3) confirm that these variables together provide the optimal explanatory power.

4.2 Comparison between ENN and ESMs predictions

Although ESMs have challenges in simulating the climatological mean ~~NPOD~~NPOG area (Fig. S2c), its long-term trend predicted by ESMs can still provide supporting evidence for our findings. There is considerable model-to-model variability in the trends of ~~NPOD~~NPOG area and its seasonal amplitude (Fig. ~~6~~7). However, the majority of models and the multi-

model average, indicate a declining trend of the ~~NPOD~~NPOG area seasonal amplitude from 2006 to 2100, qualitatively in agreement with the ENN projection.

While both ENN and ESMs indicate a decreasing trend in the amplitude of the ~~NPOD~~NPOG area seasonal cycle, the rate of 1.7 10^4 km^2 $year^{-1}$ predicted by the ESMs is slower than 3.7 10^4 km^2 $year^{-1}$ predicted by the ENN (Fig. ~~6~~7). This discrepancy can be attributed to the higher rate of expansion in the ~~NPOD~~NPOG area seasonal maximum in ESMs (Fig. ~~6~~7). The ENN predicts that the summer maximum ceases to increase after 2049 (Fig. ~~5b~~6b), which is not shown by the ESM projections (Fig. ~~S9~~S11). This likely arises from the inaccurate simulation of the North Pacific oligotrophic ocean in ESMs. The constraints on expansion of the ~~NPOD~~NPOG area seasonal maximum are not represented by ESMs in the present day (Fig. S2c), so these models will not be limited in their future expansion of the summer maximum, leading to a weaker decline in the seasonal amplitude in the ESMs. Nevertheless, the qualitative agreement between the ESMs and ENN projections gives us confidence in the ENN~~, which relies on a black box model where the underlying mechanisms are not observable.~~ prediction.

It should be noted that while ESMs provide process-based simulations, they are subject to systematic biases and model uncertainty. In biogeochemistry models within ESMs, phytoplankton growth and loss processes are usually represented through simplified empirical or semi-mechanistic parameterizations. For example, grazing is often represented as a fixed fraction of phytoplankton biomass or growth, while other losses (e.g., mortality, viral lysis) are combined into mortality terms. Such simplifications are necessary for computational efficiency, but they rely on assumptions and tuning (e.g., adjusting grazing coefficients) to reproduce observed mean chlorophyll levels (Freilich et al., 2021). Therefore, future work should aim to explicitly integrate grazing and loss processes to improve mechanistic understanding of phytoplankton accumulation dynamics. In contrast, while the ENN approach efficiently captures statistical relationships from historical data, it functions as a 'black box' with limited physical interpretability, and its predictions are constrained by the training dataset, without explicitly considering potential future changes in major oceanic features (e.g., shifts in the Kuroshio Current). Accordingly, the ENN-based simulations should be interpreted as reflecting correlations between environmental drivers and NPOG area, rather than a mechanistic representation of chlorophyll and NPOG variations.

Here, we further examine whether ESMs can capture the impact of ENSO on the ~~NPOD~~NPOG area seasonal amplitude, as proposed in Sect. 3. While previous research indicates the difficulty of ESMs in simulating ENSO processes (Bellenger et al., 2014), two models, CMCC-CESM and GISS-E2-H-CC, reveal a realistic and significant correlation between ENSO and the ~~NPOD~~NPOG area seasonal amplitude in their historical (Fig. ~~S10a,~~ S12a,b) and future (Fig. ~~S10c,~~ S12c,d) simulations. These two models simulate more pronounced declining trends in the ~~NPOD~~NPOG area seasonal amplitude than the multi-model mean (Fig. ~~6~~7), potentially indicating a physical link between ENSO and the simulated trends in ~~NPOD~~NPOG area. Moreover, in the hindcast and forecast simulations, ENSO is significantly correlated with the time series of the ~~NPOD~~NPOG area maximum in summer (Fig. ~~S10e, f, g,~~ S12e-h), in agreement with our observational findings (Fig. ~~1b~~1a).

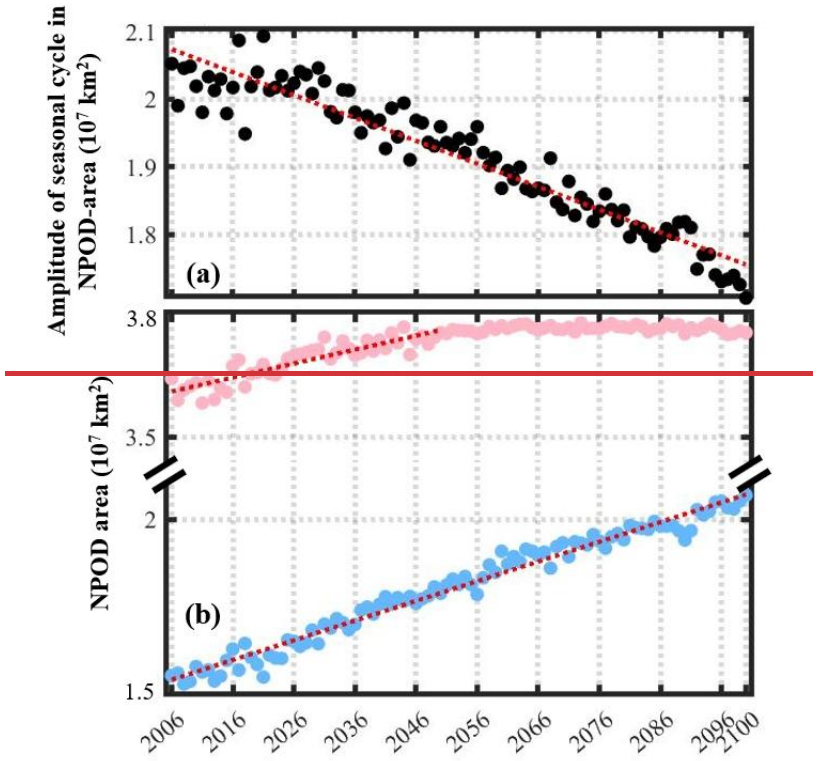
Amplitude of seasonal cycle in NPOD-area (10^7 km^2)
2.1
2
1.9
1.8
(a)
3.8
3.5
2
1.5
NPOD area (10^7 km^2)
(b)
2006
2016
2026
2036
2046
2056
2066
2076
2086
2096
2100

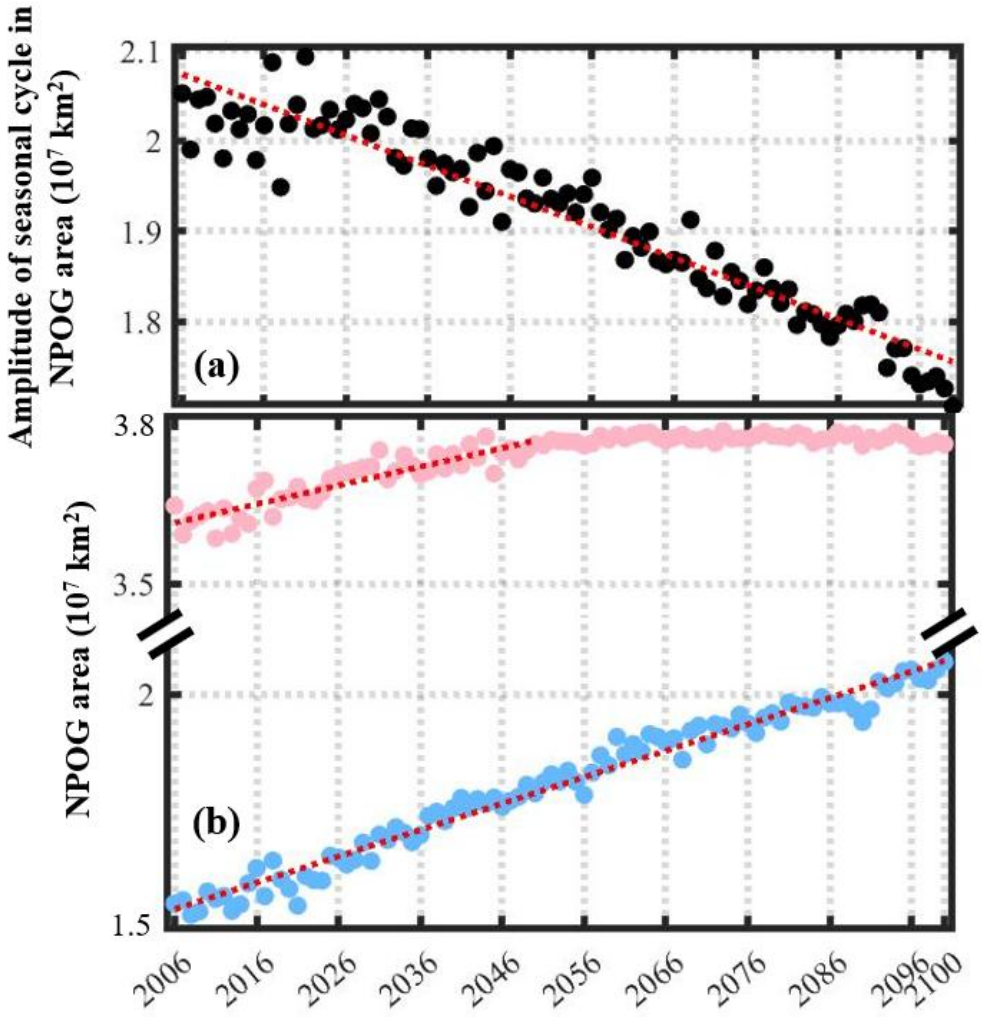

Figure ~~5~~6. Future ~~projections~~projection of ~~NPOD~~NPOG area seasonal cycle by ENN. (a-b) Time series of the seasonal amplitude (black), maximum (pink) and minimum (blue) of ~~NPOD~~NPOG area during 2006–2100 predicted by ENN.

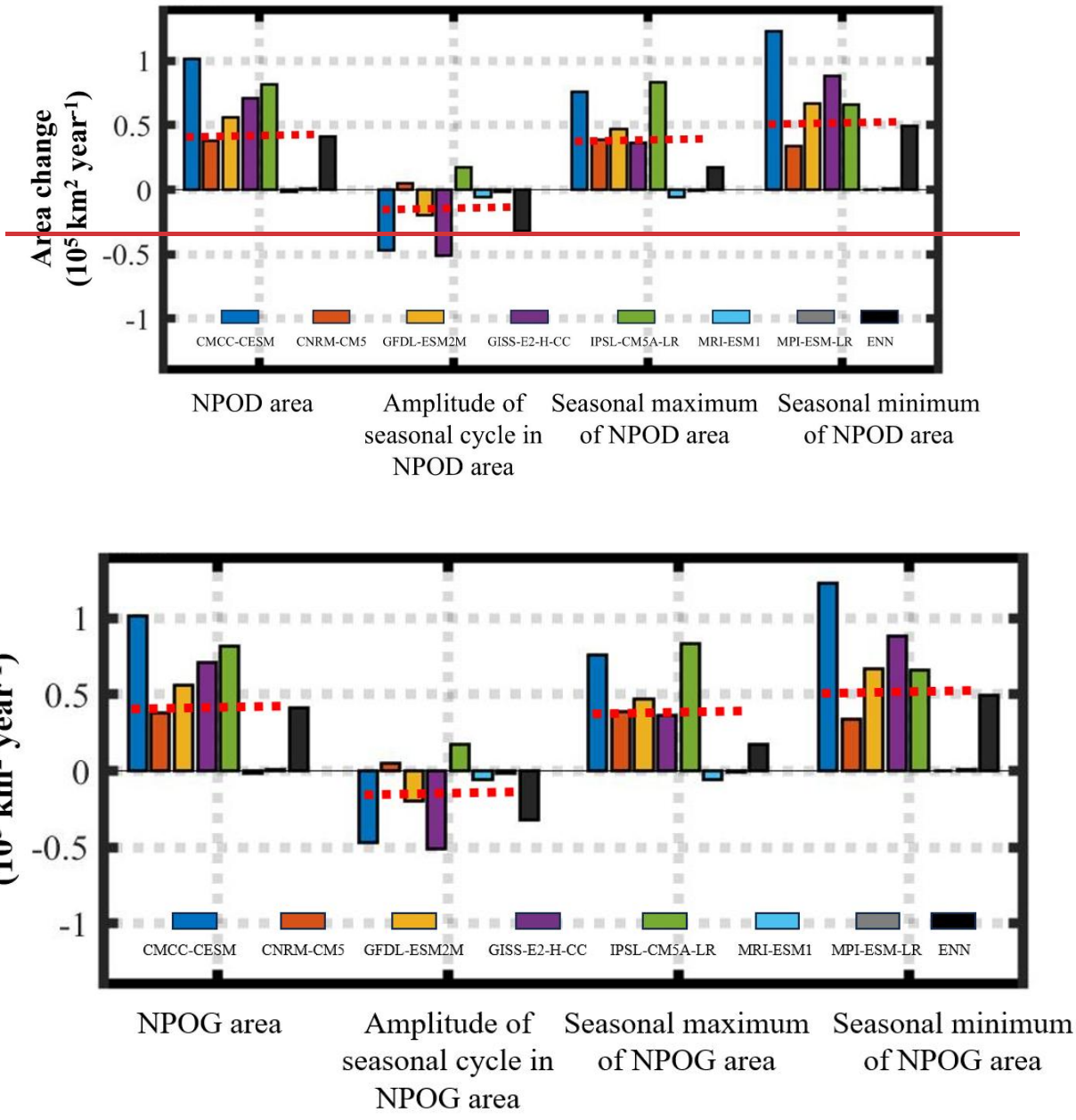

Figure ~~67~~. Comparison of future projections of ~~NPOD~~NPOG area seasonal cycle between ESMs and ENN. Variations in ~~NPOD~~NPOG area, amplitude of seasonal cycle in ~~NPOD~~NPOG area, ~~NPOD~~NPOG area seasonal maximum and minimum during 2006–2100 projected by seven ESMs in RCP 8.5 scenario and ENN (black bar). The red dashed lines represent the average across multiple ESMs.

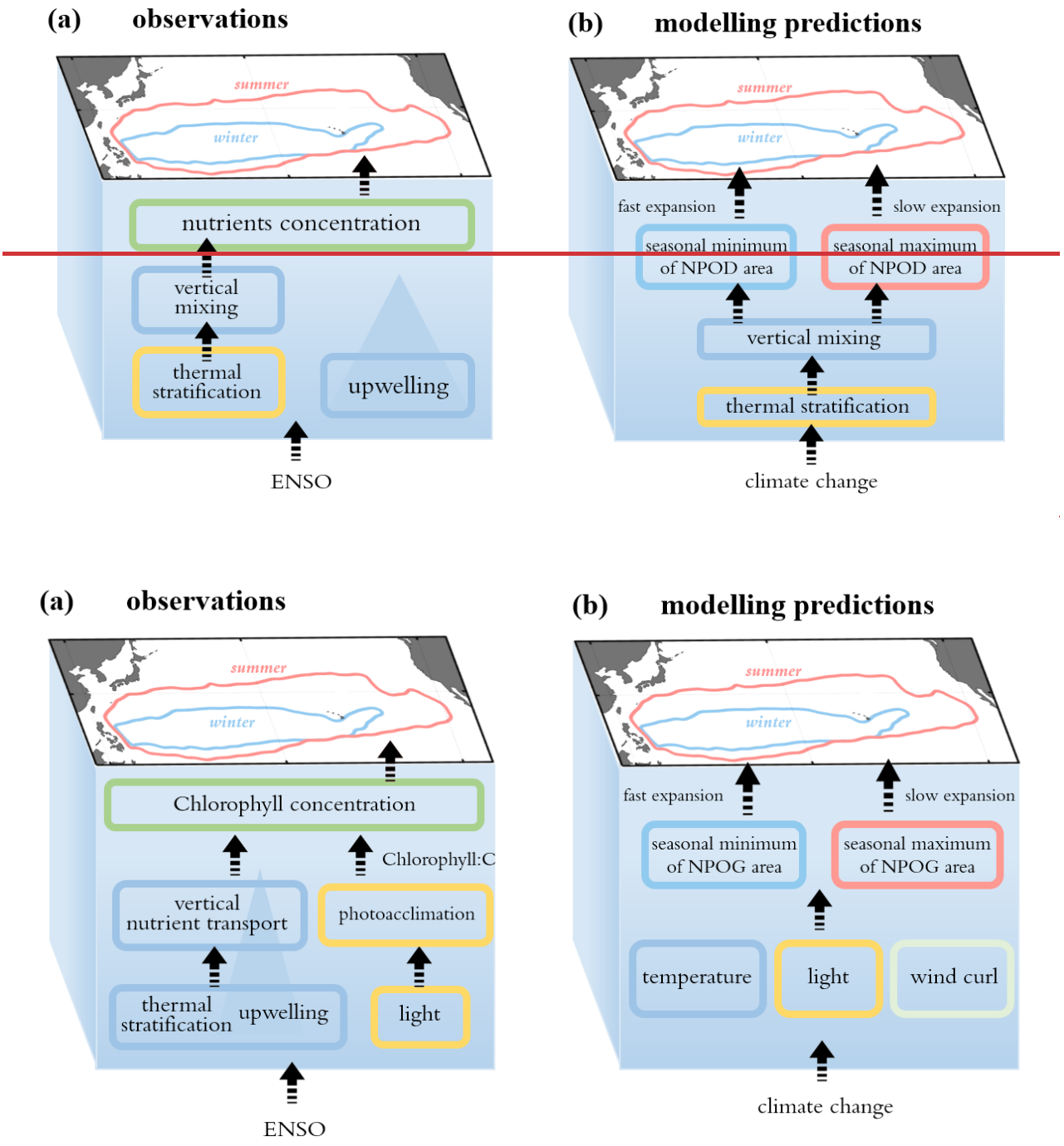

Figure ~~7~~8. Schematics of the response of ~~NPOD~~NPOG area seasonal cycle to climate processes in observations (a) and modelling predictions (b). Red curves in the geographical figures represent the seasonal maximum of ~~NPOD~~NPOG area in summer, and blue curves represent the seasonal minimum of ~~NPOD~~NPOG area in winter.

5 Conclusion

In our results, the amplitude of the seasonal cycle in ~~NPOD~~NPOG area shows interannual-scale variability without a significant trend during 1998–2021, aligned with ENSO, and the variation of the ~~NPOD~~NPOG area seasonal amplitude depends on the magnitude of the summer maximum. The impact of ENSO on the ~~NPOD~~NPOG area seasonal cycle is summarized by a schematic diagram in Fig. ~~7a~~8a. In El Niño years, ~~weak~~weaker equatorial upwelling and enhanced thermal stratification reduce ~~the vertical transfer of nutrients, finally~~nutrient supply, while higher light availability within the mixed layer induces photoacclimation, together leading to the pronounced summer expansion of ~~NPOD~~the NPOG area. Therefore, in the present day, we emphasize the dominant role of ENSO ~~-induced ocean physics~~ on ~~NPOD~~NPOG seasonality represented by the ~~NPOD~~NPOG area seasonal amplitude~~. The variation of NPOD seasonality is also linked to biogeochemical processes, such as phytoplankton photoacclimation responses, which are suggested to alter phytoplankton physiology and thus Chl a concentration in subtropical gyres (Behrenfeld et al., 2016; Dai et al., 2023; Lewandowska et al., 2014). Therefore, future work should aim to include additional datasets (e.g. in situ or experimental data) and biogeochemistry models for isolating the biogeochemical impact on NPOD separately from ocean physics~~.

Based on an ENN projection driven by CMIP5 model output, the ~~NPOD-~~NPOG area seasonal amplitude exhibits a decreasing trend over the next century due to the faster expansion of the ~~NPOD~~NPOG minimum area in winter compared to the summer maximum area (Fig. ~~7b~~8b). After the middle of the 21st century, the expansion of summer ~~NPOD~~NPOG area comes to a halt that is constrained by the boundaries of the inshore North Pacific Ocean. This constraint is absent in the CMIP5 ESMs, which consistently simulate the ~~NPOD~~NPOG to extend far further than is observed in the present day. However, this study does not account for phytoplankton dynamic processes, e.g., growth and loss, whose rates are typically two orders of magnitude greater than the changes in phytoplankton biomass.

In observations and future model projections, the interannual variation of ~~NPOD~~NPOG area is different between seasons, setting our study apart from previous research using either annual~~-~~ mean (Boyce et al., 2014; Jena et al., 2013) or deseasonalized data (Meng et al., 2021). Specifically, based on satellite observations (1998–2021), the interannual variation of the ~~NPOD~~NPOG area depends on the summer ~~NPOD-~~NPOG area maximum, as the response to climate variability. However, for future projections (2006–2100), the change of ~~NPOD~~NPOG area is determined by the winter ~~NPOD-~~NPOG area minimum, reflecting the response to anthropogenic climate change. Therefore, it is essential for future analyses of ~~NPOD~~NPOG expansion to consider this seasonal difference, as the varying expansion rates of ~~NPOD~~NPOG in different seasons have significant implications for the season-dependent fisheries (Muñiz et al., 2021) and the Pacific ecosystems (Bidigare et al., 2009; Yoo et al., 2008).

~~NPOD~~NPOG seasonality is influenced by both interannual climate variability and long-term climate change, with the dominant process determined by the time scales. On a decadal scale, the PDO and North Pacific Gyre Oscillation (NPGO) may also impact ~~NPOD~~NPOG seasonality by altering the ~~intensity of the~~ gyre circulations~~ and nutrients~~, nutrient transport and phytoplankton phenology (Di Lorenzo et al., 2008; Meng et al., 2021). Although progress has been made in

understanding the relationships between ~~NPOD~~NPOG variations and climate processes, there is still a challenge for future studies to separate the contribution of contemporary climate variability and anthropogenic climate change. Such a partitioning will significantly refine our understanding of ocean ecosystem responses to climate.

Code availability

The ENN code and the code used for generating the figures are available in the online repository Zenodo and can be accessed via the following link: https://zenodo.org/records/14632256 (Meng et al., 2025).

Data availability

The data used to generate the figures are available in the Zenodo online repository at https://zenodo.org/records/14632256 (Meng et al., 2025). Detailed source data and the corresponding link are provided in Text S2.

Supplement

The supplement is available on the BG submission system

Author contributions

SM designed the methodology, developed the software, conducted the analysis and investigation, and prepared the manuscript with contributions from all co-authors. Xun Gong contributed to validation, analysis, and resources. BW and MJ reviewed and edited the manuscript. XD supported formal analysis, while Xiang Gong contributed to the methodology. MG handled data curation. HG oversaw the project, provided funding, and guided the research.

Competing interests

The authors declare that they have no conflict of interest.

Acknowledgments

We thank NASA OBPG for providing satellite data. We acknowledge the Working Group on Coupled Modelling (WGCM) and the climate modelling groups (listed in Table S2) for their model output.

Financial support

This work is funded by the NSFC-Shandong Joint Fund (U1906215); Ministry of Science and Technology of the People's Republic of China (2019YFE0125000); National Nature Science Foundation of China (41876125); State Key Laboratory of Biogeology and Environmental Geology, China University of Geosciences (GKZ22Y656); Jinan Science and Technology Bureau (202228034); Major Scientific Research Project for the Construction of State Key Laboratory at Qilu University of Technology (Shandong Academy of Sciences) (2025ZDGZ01).

References

An, S. I. and Wang, B.: Mechanisms of locking of the El Niño and La Niña mature phases to boreal winter, J Clim, 14, 2164–2176, https://doi.org/10.1175/1520-0442(2001)014<2164:MOLOTE>2.0.CO;2, 2001.

Barber, R. T. and Chavez, F. P.: Biological consequences of El Niño, Science (1979), 222, 1203–1210, https://doi.org/10.1126/science.222.4629.1203, 1983.

Behrenfeld, M. J., Boss, E., Siegel, D. A., and Shea, D. M.: Carbon-based ocean productivity and phytoplankton physiology from space, Global Biogeochem Cycles, 19, 1–14, https://doi.org/10.1029/2004GB002299, 2005.

Behrenfeld, M. J., O'Malley, R. T., Siegel, D. A., McClain, C. R., Sarmiento, J. L., Feldman, G. C., Milligan, A. J., Falkowski, P. G., Letelier, R. M., and Boss, E. S.: Climate-driven trends in contemporary ocean productivity, Nature, 444, 752–755, https://doi.org/10.1038/nature05317, 2006.

Behrenfeld, M. J., O'Malley, R. T., Boss, E. S., Westberry, T. K., Graff, J. R., Halsey, K. H., Milligan, A. J., Siegel, D. A., and Brown, M. B.: Revaluating ocean warming impacts on global phytoplankton, Nat Clim Chang, 6, 323–330, https://doi.org/10.1038/NCLIMATE2838, 2016.

Bellenger, H., Guilyardi, E., Leloup, J., Lengaigne, M., and Vialard, J.: ENSO representation in climate models: from CMIP3 to CMIP5, Clim Dyn, 42, 1999–2018, https://doi.org/10.1007/s00382-013-1783-z, 2014.

Bidigare, R. R., Chai, F., Landry, M. R., Lukas, R., Hannides, C. C. S., Christensen, S. J., Karl, D. M., Shi, L., and Chao, Y.: Subtropical ocean ecosystem structure changes forced by North Pacific climate variations, J Plankton Res, 31, 1131–1139, https://doi.org/10.1093/plankt/fbp064, 2009.

Boyce, D. G., Dowd, M., Lewis, M. R., and Worm, B.: Estimating global chlorophyll changes over the past century, Prog Oceanogr, 122, 163–173, https://doi.org/10.1016/j.pocean.2014.01.004, 2014.

Carton, J. A., Chepurin, G. A., and Chen, L.: SODA3: A new ocean climate reanalysis, J Clim, 31, 6967–6983, https://doi.org/10.1175/JCLI-D-18-0149.1, 2018.

Chow, C. H., Cheah, W., Tai, J. H., and Liu, S. F.: Anomalous wind triggered the largest phytoplankton bloom in the oligotrophic North Pacific Subtropical Gyre, Sci Rep, 9, 15550, https://doi.org/10.1038/s41598-019-51989-x, 2019.

Cole, H., Henson, S., Martin, A., and Yool, A.: Mind the gap: The impact of missing data on the calculation of phytoplankton phenology metrics, J Geophys Res Oceans, 117, C8030, https://doi.org/10.1029/2012JC008249, 2012.

Dai, M., Luo, Y. W., Achterberg, E. P., Browning, T. J., Cai, Y., Cao, Z., Chai, F., Chen, B., Church, M. J., Ci, D., Du, C., Gao, K., Guo, X., Hu, Z., Kao, S. J., Laws, E. A., Lee, Z., Lin, H., Liu, Q., Liu, X., Luo, W., Meng, F., Shang, S., Shi, D., Saito, H., Song, L., Wan, X. S., Wang, Y., Wang, W. L., Wen, Z., Xiu, P., Zhang, J., Zhang, R., and Zhou, K.: Upper ocean biogeochemistry of the oligotrophic North Pacific Subtropical Gyre: From nutrient sources to carbon export, Reviews of Geophysics, 61, e2022RG000800, https://doi.org/10.1029/2022RG000800, 2023.

Di Lorenzo, E., Schneider, N., Cobb, K. M., Franks, P. J. S., Chhak, K., Miller, A. J., McWilliams, J. C., Bograd, S. J., Arango, H., Curchitser, E., Powell, T. M., and Rivière, P.: North Pacific Gyre Oscillation links ocean climate and ecosystem change, Geophys Res Lett, 35, 2007GL032838, https://doi.org/10.1029/2007GL032838, 2008.

Dore, J. E., Letelier, R. M., Church, M. J., Lukas, R., and Karl, D. M.: Summer phytoplankton blooms in the oligotrophic North Pacific Subtropical Gyre: Historical perspective and recent observations, Prog Oceanogr, 76, 2–38, https://doi.org/10.1016/j.pocean.2007.10.002, 2008.

Elman, J. L.: Finding structure in time, Cogn Sci, 14, 179–211, https://doi.org/10.1207/s15516709cog1402_1, 1990.

Feng, Y., Chen, X., and Tung, K.-K.: ENSO diversity and the recent appearance of Central Pacific ENSO, Clim Dyn, 54, 413–433, https://doi.org/10.1007/s00382-019-05005-7, 2020.

Fu, W., Moore, J. K., Primeau, F., Collier Nathan and Ogunro, O. O., Hoffman, F. M., and Randerson, J. T.: Evaluation of ocean biogeochemistry and carbon cycling in CMIP Earth System Models with the International Ocean Model Benchmarking (IOMB) software system, J Geophys Res Oceans, 127, e2022JC018965, https://doi.org/10.1029/2022JC018965, 2022.

Gregg, W. W. and Rousseaux, C. S.: Decadal trends in global pelagic ocean chlorophyll: A new assessment integrating multiple satellites, in situ data, and models, J Geophys Res Oceans, 119, 5921–5933, https://doi.org/10.1002/2014JC010158, 2014.

Henson, S., Cole, H., Beaulieu, C., and Yool, A.: The impact of global warming on seasonality of ocean primary production, Biogeosciences, 10, 1421–1450, https://doi.org/10.5194/bgd-10-1421-2013, 2013.

Henson, S. A., Sarmiento, J. L., Dunne, J. P., Bopp, L., Lima, I., Doney, S. C., John, J., and Beaulieu, C.: Detection of anthropogenic climate change in satellite records of ocean chlorophyll and productivity, Biogeosciences, 7, 621–640, https://doi.org/10.5194/bg-7-621-2010, 2010.

Hersbach, H., Bell, B., Berrisford, P., Biavati, G., Horányi, A., Muñoz Sabater, J., Nicolas, J., Peubey, C., Radu, R., Rozum, I., Schepers, D., Simmons, A., Soci, C., Dee, D., and Thépaut, J-N.: ERA5 monthly averaged data on single levels from 1940 to present [dataset], https://doi.org/10.24381/cds.f17050d7, 2023.

Irwin, A. J. and Oliver, M. J.: Are ocean deserts getting larger?, Geophys Res Lett, 36, 2009GL039883, https://doi.org/10.1029/2009GL039883, 2009.

Itoh, S., Yasuda, I., Saito, H., and Tsuda Atsushi and Komatsu, K.: Mixed layer depth and chlorophyll *a*: Profiling float observations in the Kuroshio-Oyashio Extension region, Journal of Marine Systems, 151, 1–14, https://doi.org/10.1016/j.jmarsys.2015.06.004, 2015.

Jacox, M. G., Fiechter, J., Moore, A. M., and Edwards, C. A.: ENSO and the California current coastal upwelling response, J Geophys Res Oceans, 120, 1691–1702, https://doi.org/10.1002/2014JC010650, 2015.

Jena, B., Sahu, S., Avinash, K., and Swain, D.: Observation of oligotrophic gyre variability in the south Indian Ocean: Environmental forcing and biological response, Deep Sea Res 1 Oceanogr Res Pap, 80, 1–10, https://doi.org/10.1016/j.dsr.2013.06.002, 2013.

Kwiatkowski, L., Bopp, L., Aumont, O., Ciais, P., Cox, P. M., Laufkotter, C., Li, Y., and Seferian, R.: Emergent constraints on projections of declining primary production in the tropical oceans, Nat Clim Chang, 7, 355–358, https://doi.org/10.1038/NCLIMATE3265, 2017.

Large, W. G., Mcwilliams, J. C., and Doney, S. C.: Oceanic vertical mixing: A review and a model with a nonlocal boundary layer parameterization, Reviews of Geophysics, 32, 363–403, https://doi.org/10.1029/94RG01872, 1994.

Laws, E. A.: Evaluation of in situ phytoplankton growth rates: A synthesis of data from varied approaches, Ann Rev Mar Sci, 5, 247–268, https://doi.org/10.1146/annurev-marine-121211-172258, 2013.

Leonelli, F. E., Bellacicco, M., Pitarch, J., Organelli, E., Nardelli, B. B., de Toma, V., Cammarota, C., and Marullo S. and Santoleri, R.: Ultra-oligotrophic waters expansion in the North Atlantic Subtropical Gyre revealed by 21 Years of satellite observations, Geophys Res Lett, 49, 2021GL096965, https://doi.org/10.1029/2021GL096965, 2022.

Lewandowska, A. M., Boyce, D. G., Hofmann Matthias and Matthiessen, B., Sommer, U., and Worm, B.: Effects of sea surface warming on marine plankton, Ecol Lett, 17, 614–623, https://doi.org/10.1111/ele.12265, 2014.

~~Levitus, S.: NODC Standard Product: World ocean atlas 2005 (4 disc set) [dataset], https://www.ncei.noaa.gov/access/metadata/landing-page/bin/iso?id=gov.noaa.nodc:0097967, 2013.~~

Lin, P., Chai, F., Xue, H., and Xiu, P.: Modulation of decadal oscillation on surface chlorophyll in the Kuroshio Extension, J Geophys Res Oceans, 119, 187–199, https://doi.org/10.1002/2013JC009359, 2014.

Di Lorenzo, E., Schneider, N., Cobb, K. M., Franks, P. J. S., Chhak, K., Miller, A. J., McWilliams, J. C., Bograd, S. J., Arango, H., Curchitser, E., Powell, T. M., and Rivière, P.: North Pacific Gyre Oscillation links ocean climate and ecosystem change, Geophys Res Lett, 35, 2007GL032838, https://doi.org/10.1029/2007GL032838, 2008.

Lozier, M. S., Dave, A. C., Palter, J. B., Gerber, L. M., and Barber, R. T.: On the relationship between stratification and primary productivity in the North Atlantic, Geophys Res Lett, 38, 2011GL049414, https://doi.org/10.1029/2011GL049414, 2011.

Lutz, M. J., Caldeira, K., Dunbar, R. B., and Behrenfeld, M. J.: Seasonal rhythms of net primary production and particulate organic carbon flux to depth describe the efficiency of biological pump in the global ocean, J Geophys Res Oceans, 112, ~~2006JC003706,~~ https://doi.org/10.1029/2006JC003706, 2007.

Mao, Z., Mao, Z., Jamet, C., Linderman, M., Wang, Y., and Chen, X.: Seasonal cycles of phytoplankton expressed by sine equations using the daily climatology from satellite-retrieved chlorophyll-a concentration (1997–2019) over global ocean, Remote Sens (Basel), 12, 2662, https://doi.org/10.3390/rs12162662, 2020.

Martinez, E., Antoine, D., D'Ortenzio, F., and Gentili, B.: Climate-driven basin-scale decadal oscillations of oceanic phytoplankton, Science (1979), 326, 1253–1256, https://doi.org/10.1126/science.1177012, 2009.

McClain, C. R., Signorini, S. R., and Christian, J. R.: Subtropical gyre variability observed by ocean-color satellites, Deep Sea Res 2 Top Stud Oceanogr, 51, 281–301, https://doi.org/10.1016/j.dsr2.2003.08.002, 2004.

Meng, S., Gong, X., Yu, Y., Yao, X., Gong, X., Lu, K., Zhang, C., Shi, J., Yu, X., and Gao, H.: Strengthened ocean-desert process in the North Pacific over the past two decades, Environmental Research Letters, 16, 24–34, https://doi.org/10.1088/1748-9326/abd96f, 2021.

Meng, S.: Data for "Seasonality of the North Pacific Ocean Desert area in the past two decades and a modelling perspective for the 21st century" [dataset], https://zenodo.org/records/14632256, 2025.

Moss, R. H., Edmonds, J. A., Hibbard, K. A., Manning, M. R., Rose, S. K., van Vuuren, D. P., Carter, T. R., Emori, S., Kainuma, M., Kram, T., Meehl, G. A., Mitchell, J. F. B., Nakicenovic, N., Riahi, K., Smith, S. J., Stouffer, R. J., Thomson, A. M., Weyant, J. P., and Wilbanks, T. J.: The next generation of scenarios for climate change research and assessment, Nature, 463, 747–756, https://doi.org/10.1038/nature08823, 2010.

Muñiz, C., McQuaid, C. D., and Weidberg, N.: Seasonality of primary productivity affects coastal species more than its magnitude, Science of the Total Environment, 757, 143740, https://doi.org/10.1016/j.scitotenv.2020.143740, 2021.

NASA Goddard Space Flight Center, Ocean Ecology Laboratory, Ocean Biology Processing Group (OBPG): MODIS-aqua ocean color data [dataset], https://doi.org/10.5067/AQUA/MODIS/L3M/SST/2014, 2014.

Pennington, J. T., Mahoney, K. L., Kuwahara, V. S., Kolber, D. D., Calienes, R., and Chavez, F. P.: Primary production in the eastern tropical Pacific: A review, Prog Oceanogr, 69, 285–317, https://doi.org/10.1016/j.pocean.2006.03.012, 2006.

Polovina, J. J., Howell, E. A., and Abecassis, M.: Ocean's least productive waters are expanding, Geophys Res Lett, 35, 2007GL0317455, https://doi.org/10.1029/2007GL031745, 2008.

Racault, M.-F., Sathyendranath, S., Brewin Robert J. W. and Raitsos, D. E., Jackson, T., and Platt, T.: Impact of El Niño variability on oceanic phytoplankton, Front Mar Sci, 4, 133, https://doi.org/10.3389/fmars.2017.00133, 2017.

Raes, E. J., Hörstmann, C., Landry, M. R., Beckley, L. E., Marin, M., Thompson, P., Antoine, D., Focardi, A., O'Brien, J., Ostrowski, M., and Waite, A. M.: Dynamic change in an ocean desert: Microbial diversity and trophic transfer along the 110 °E meridional in the Indian Ocean, Deep Sea Res 2 Top Stud Oceanogr, 201, 105097, https://doi.org/10.1016/j.dsr2.2022.105097, 2022.

Rayner, N. A., Parker, D. E., Horton, E. B., Folland, C. K., Alexander, L., Rowell, D. P., Kent, E. C., and Kaplan, A.: Global analyses of sea surface temperature, sea ice, and night marine air temperature since the late nineteenth century, Journal of Geophysical Research: Atmospheres, 108, 2002JD002670JOURNAL OF GEOPHYSICAL RESEARCH-ATMOSPHERES, 108, https://doi.org/10.1029/2002JD002670, 2003.

Reynolds, R. W.: A real-time global sea surface temperature analysis, J Clim, 1, 75–86, https://doi.org/10.1175/1520-0442(1988)001<0075:ARTGSS>2.0.CO;2, 1988.

Schwalm, C. R., Glendon, S., and Duffy, P. B.: RCP8.5 tracks cumulative CO2 emissions, Proc Natl Acad Sci U S A, 117, 19656–19657, https://doi.org/10.1073/pnas.2007117117, 2020.

Séférian, R., Bopp, L., Gehlen, M., Orr, J. C., Ethé, C., Cadule, P., Aumont, O., Salas y Mélia, D., Voldoire, A., and Madec, G.: Skill assessment of three earth system models with common marine biogeochemistry, Clim Dyn, 40, 2549–2573, https://doi.org/10.1007/s00382-012-1362-8, 2013.

Signorini, S. R. and McClain, C. R.: Subtropical gyre variability as seen from satellites, Remote Sensing Letters, 3, ~~625053,~~ https://doi.org/10.1080/01431161.2011.625053, 2012.

Signorini, S. R., Franz, B. A., and McClain, C. R.: Chlorophyll variability in the oligotrophic gyres: Mechanisms, seasonality and trends, Front Mar Sci, 2, https://doi.org/10.3389/fmars.2015.00001, 2015.

Stock, A., Crowder, L. B., Halpern, B. S., and Micheli, F.: Uncertainty analysis and robust areas of high and low modeled human impact on the global oceans, Conservation Biology, 32, 1368–1379, https://doi.org/10.1111/cobi.13141, 2018.

Taylor, K. E., Stouffer, R. J., and Meehl, G. A.: An overview of CMIP5 and the experiment design, Bull Am Meteorol Soc, 93, 485–498, https://doi.org/10.1175/BAMS-D-11-00094.1, 2012.

Tian, F. and Zhang, R. H.: Emerging hotspots of surface chlorophyll trend in the Tropical Oceans, J Geophys Res Oceans, 129, 2023JC020681, https://doi.org/10.1029/2023JC020681, 2024.

Toyoda, T. and Okamoto, S.: Physical forcing of late summer chlorophyll a blooms in the oligotrophic eastern North Pacific, J Geophys Res Oceans, 122, 1849–1861, https://doi.org/10.1002/2016JC012423, 2017.

Villareal, T. A., Adornato, L., Wilson, C., and Schoenbaechler, C. A.: Summer blooms of diatom-diazotroph assemblages and surface chlorophyll in the North Pacific gyre: A disconnect, J Geophys Res Oceans, 116, 2010JC006268, https://doi.org/10.1029/2010JC006268, 2011.

Villareal, T. A., Brown, C. G., Brzezinski, M. A., Krause, J. W., and Wilson, C.: Summer diatom blooms in the north Pacific subtropical gyre: 2008-2009, PLoS One, 7, e33109, https://doi.org/10.1371/journal.pone.0033109, 2012.

Wilson, C. and Qiu, X.: Global distribution of summer chlorophyll blooms in the oligotrophic gyres, Prog Oceanogr, 78, 107–134, https://doi.org/10.1016/j.pocean.2008.05.002, 2008.

Wilson, C., Villareal, T. A., Brzezinski, M. A., Krause, J. W., and Shcherbina, A. Y.: Chlorophyll bloom development and the subtropical front in the North Pacific, J Geophys Res Oceans, 118, 1473–1488, https://doi.org/10.1002/jgrc.20143, 2013.

Wu, R. G. and Kirtman, B. P.: Near-annual SST variability in the Equatorial Pacific in a coupled general circulation model, J Clim, 18, 4454–4473, https://doi.org/10.1175/JCLI3536.1, 2005.

Yamaguchi, R. and Suga, T.: Trend and variability in global upper-ocean stratification since the 1960s, J Geophys Res Oceans, 124, 8933–8948, https://doi.org/10.1029/2019JC015439, 2019.

Yoo, S., Batchelder, H. P., Peterson, W. T., and Sydeman, W. J.: Seasonal, interannual and event scale variation in North Pacific ecosystems, Prog Oceanogr, 77, 155–181, https://doi.org/10.1016/j.pocean.2008.03.013, 2008.

Zuo, H., Balmaseda, M. A., Tietsche, S., Mogensen, K., and Mayer, M.: The ECMWF operational ensemble reanalysis-analysis system for ocean and sea ice: A description of the system and assessment, Ocean Science, 15, https://doi.org/10.5194/os-15-779-2019, 2019.